Nuclear Energy in Central Europe '99
Portorož, Slovenia, 6 to 9 September, 1999

A Combined Single-Multiphase Flow Formulation of the Premixing Phase Using the Level Set Method

Matjaž Leskovar[1], Jure Marn[2]
[1] "Jožef Stefan" Institute, Jamova 39, 1000 Ljubljana, Slovenia
[2]Fakulteta za strojništvo, Smetanova 17, 2000 Maribor, Slovenia

ABSTRACT – The premixing phase of a steam explosion covers the interaction of the melt jet or droplets with the water prior to any steam explosion occurring. To get a better insight of the hydrodynamic processes during the premixing phase beside hot premixing experiments, where the water evaporation is significant, also cold isothermal premixing experiments are performed.

The speciality of isothermal premixing experiments is that three phases are involved: the water, the air and the spheres phase, but only the spheres phase mixes with the other two phases, whereas the water and air phases do not mix and remain separated by a free surface. Our idea therefore was to treat the isothermal premixing process with a combined single-multiphase flow model. In this combined model the water and air phase are treated as a single phase with discontinuous phase properties at the water-air interface, whereas the spheres are treated as usually with a multiphase flow model, where the spheres represent the dispersed phase and the common water-air phase represents the continuous phase.

The common water-air phase was described with the front capturing method based on the level set formulation. In the level set formulation, the boundary of two-fluid interfaces is modeled as the zero set of a smooth signed normal distance function defined on the entire physical domain. The boundary is then updated by solving a nonlinear equation of the Hamilton-Jacobi type on the whole domain.

With this single-multiphase flow model the Queos isothermal premixing experiment Q08 has been simulated. A numerical analysis using different treatments of the water-air interface (level set, high-resolution and upwind) has been performed for the incompressible and compressible case and the results were compared to experimental measurements.

Nomenclature

a,b,c	derivatives
d	diameter, distance or derivative
$\vec{\mathbf{g}}$	gravity
G	expression
Δh	mesh size
Δl	characteristic length
m	mass
M	number of mesh points
$\vec{\mathbf{M}}$	friction
$\vec{\mathbf{r}}$	coordinate
$sign$	sign function
t	time
Δt	iteration time step
T	temperature
$\vec{\mathbf{v}}$	velocity
p	pressure

Greek Letters

α	phase presence probability
ε	interface thickness
ϕ	level set function, mass flow rate
λ	thermal conductivity
ρ	density

Subscripts / Superscripts

0	initial level set function
a,s,w	air, spheres, water phase
b,s	boundary, water surface
c,d	continuous, dispersed
j,l	spatial coordinate
n	time step, number of iterations
p	phase
r,z	coordinate

1. Introduction

The premixing phase of a steam explosion covers the interaction of the melt jet or droplets with water prior to any steam explosion occurring. The form of the premixture determines the coolability of the resulting debris and gives the initial conditions of the possible steam explosion. To get a better insight of the hydrodynamic processes during the premixing phase beside hot premixing experiments, where the water evaporation is significant, also cold isothermal premixing experiments are performed. In these isothermal premixing experiments different jets of spheres are injected in a water pool [1].

The speciality of isothermal premixing experiments is that three phases are involved: the water, the air and the spheres phase, but only the spheres phase mixes with the other two phases, whereas the water and air phases do not mix and remain separated by a free surface. Our idea therefore was to treat the isothermal premixing process with a combined single-multiphase flow model. In this combined model the water and air phase are treated as a single phase with discontinuous phase properties at the water-air interface, whereas the spheres are treated as usually with a multiphase flow model [2], where the spheres represent the dispersed phase and the common water-air phase represents the continuous phase.

2. Governing Equations

Each phase p in the multiphase flow – the continuous common water-air phase $p = c$ and the dispersed spheres phase $p = d$ – is described using the probabilistic mass

$$\frac{\partial(\alpha_p \rho_p)}{\partial t} + \nabla \cdot (\alpha_p \rho_p \vec{\mathbf{v}}_p) = 0 \tag{1}$$

and momentum equations

$$\rho_p \frac{\partial \vec{\mathbf{v}}_p}{\partial t} + \rho_p (\vec{\mathbf{v}}_p \cdot \nabla) \vec{\mathbf{v}}_p = -\nabla p + \rho_p \vec{\mathbf{g}} + \vec{\mathbf{M}}_p \tag{2}$$

obtained by ensemble averaging. The interfacial friction force $\vec{\mathbf{M}}$ is defined as

$$\vec{\mathbf{M}}_d = \vec{\mathbf{M}}_d^{drag} + \vec{\mathbf{M}}_d^{vm} + \vec{\mathbf{M}}_d^{lift}, \quad \alpha_c \vec{\mathbf{M}}_c = -\alpha_d \vec{\mathbf{M}}_d, \tag{3}$$

where the drag force is calculated from [3]

$$\vec{\mathbf{M}}_d^{drag} = 0.44 \cdot \frac{3}{4} \frac{\alpha_d \rho_c}{d_d} |\vec{\mathbf{v}}_c - \vec{\mathbf{v}}_d| (\vec{\mathbf{v}}_c - \vec{\mathbf{v}}_d), \tag{4}$$

the virtual mass force from [3]

$$\vec{\mathbf{M}}_d^{vm} = 0.5 \alpha_d \rho_c \left(\frac{D\vec{\mathbf{v}}_c}{Dt} - \frac{D\vec{\mathbf{v}}_d}{Dt} \right) \tag{5}$$

and the lift force from [3]

$$\vec{\mathbf{M}}_d^{lift} = 0.5 \alpha_d \rho_c (\vec{\mathbf{v}}_c - \vec{\mathbf{v}}_d) \times (\nabla \times \vec{\mathbf{v}}_c). \tag{6}$$

The pressure equation for the assumed common pressure field p was derived from the sum of the conservative form of the compressible flow continuity equation (1) over all phases using the projection method

$$\sum_p \left(\frac{\alpha_p^{n+1}}{\rho_p^n} \frac{\partial \rho}{\partial p} (p^{n+1} - p^n) + \nabla \cdot (\alpha_p^{n+1} \vec{\mathbf{v}}_p^{n+1/2}) \Delta t - \nabla \cdot \left(\alpha_p^{n+1} \frac{1}{\rho_p^{n+1}} \nabla p^{n+1} \right) \Delta t \right) = 0, \tag{7}$$

where

$$\vec{\mathbf{v}}_p^{n+1/2} = \vec{\mathbf{v}}_p^n - \Delta t (\vec{\mathbf{v}}_p^n \cdot \nabla) \vec{\mathbf{v}}_p^n \tag{8}$$

and

$$\rho_c^{n+1} = \frac{\alpha_w^{n+1}\rho_w^n + \alpha_a^{n+1}\rho_a^n}{\alpha_w^{n+1} + \alpha_a^{n+1}}, \quad \rho_d^{n+1} = \rho_s^n . \tag{9}$$

3. Level Set Method

There are two types of numerical approaches for solving free surface problems. One is based on front tracking where the free interfaces are explicitly tracked and the second is based on front capturing. The drawback of the front tracking methods is that they are difficult to continue beyond the singularity time when the interface forms a singularity or changes its topology. For our combined single-multiphase flow model we therefore chose the front capturing method based on a level set formulation which is widely used in the last years [4].

In the level set formulation, the boundary of two-fluid interfaces is modeled as the zero set of a smooth signed normal distance function $\phi = 0$ defined on the entire physical domain as $\phi(\vec{\mathbf{r}}, t=0) = \pm d(\vec{\mathbf{r}})$, where $d(\vec{\mathbf{r}})$ is the signed minimal distance from the two-fluid interface at the initial time $t = 0$. The boundary position is then updated by solving a nonlinear equation of the Hamilton-Jacobi type on the whole domain

$$\frac{\partial \phi}{\partial t} + (\vec{\mathbf{v}} \cdot \nabla)\phi = 0, \tag{10}$$

which moves the zero level of ϕ exactly as the actual two-fluid interface moves. Such a level set formulation of the moving interface is capable of computing geometric properties of highly complicated boundaries without explicitly tracking the interface. Hence, the moving boundary can develop corners, cusps, and undergo topological changes quite naturally. The problems of grid surgery encountered in the tracking approach are so eliminated. Since ϕ is a smooth function, unlike the fluid density ρ, which undergoes a jump at the two-fluid interface, the level set equation (10) is more easily solved numerically.

The density of the common water-air phase is determined by the level set function as

$$\rho(\phi) = \begin{cases} \rho_w, & \phi > 0 \\ (\rho_w + \rho_a)/2, & \phi = 0 . \\ \rho_a, & \phi < 0 \end{cases} \tag{11}$$

If this prescription is used straightforward a graded solution will be produced and instabilities will occur, especially for large density ratios. Therefore it is desirable to smooth the density at the interface with

$$\rho(\phi) = \begin{cases} \rho_w, & \phi > \varepsilon \\ \dfrac{(\rho_w + \rho_a)}{2} + \dfrac{(\rho_w - \rho_a)}{2}\left(\dfrac{\phi}{\varepsilon} + \dfrac{1}{\pi}\sin\left(\dfrac{\pi\phi}{\varepsilon}\right)\right), & |\phi| \le \varepsilon , \\ \rho_a, & \phi < -\varepsilon \end{cases} \tag{12}$$

where ε is the prescribed interface thickness as long as ϕ is a distance function. In our computations we used $\varepsilon = \frac{3}{2}\Delta h$.

It should be noted that while ϕ is initially a distance function it will not remain so at later times since the level set equation (10) deforms it. To maintain the interface thickness fixed in time the level set function ϕ has to be reinitialised at each time step so that it remains a distance function. The reinitialisation is carried out by solving the equation

$$\frac{\partial \phi}{\partial t} = sign(\phi_0)(1 - |\nabla\phi|), \quad \phi(\vec{\mathbf{r}}, 0) = \phi_0(\vec{\mathbf{r}}) \tag{13}$$

for the steady state solution, where ϕ_0 is the calculated level set function at time t. The solution of equation (13) will have the same sign and the same zero level set as ϕ_0, and since it satisfies $|\nabla\phi| = 1$, it will be a distance function. The steady state solution of the reinitialisation equation (13) was numerically obtained with the following iteration procedure:

$$\phi_{j,l}^{n+1} = \phi_{j,l}^{n} + \Delta t \, sign(\phi_{0\,j,l})(1 - G_{j,l}), \tag{14}$$

where $G_{j,l}$ is defined as

$$G_{j,l} = \begin{cases} \sqrt{\max\left((a_{j,l}^{+})^2, (b_{j,l}^{-})^2\right) + \max\left((c_{j,l}^{+})^2, (d_{j,l}^{-})^2\right)}, & \phi_{0\,j,l} \geq 0.5\Delta h \\ \sqrt{\max\left((a_{j,l}^{-})^2, (b_{j,l}^{+})^2\right) + \max\left((c_{j,l}^{-})^2, (d_{j,l}^{+})^2\right)}, & \phi_{0\,j,l} \leq -0.5\Delta h \\ 1, & -0.5\Delta h < \phi_{0\,j,l} < 0.5\Delta h \end{cases}, \tag{15}$$

with

$$\begin{aligned} a_{j,l} &= (\phi_{j,l} - \phi_{j-1,l})/\Delta h, \\ b_{j,l} &= (\phi_{j+1,l} - \phi_{j,l})/\Delta h, \\ c_{j,l} &= (\phi_{j,l} - \phi_{j,l-1})/\Delta h, \\ d_{j,l} &= (\phi_{j,l+1} - \phi_{j,l})/\Delta h \end{aligned} \tag{16}$$

and

$$a^{+} = \max(0, a), \quad a^{-} = \min(0, a). \tag{17}$$

The stopping criterion for the iteration of the steady state solution was

$$\sum_{|\phi_{j,l}^{n}| < \varepsilon} |\phi_{j,l}^{n+1} - \phi_{j,l}^{n}| < \Delta t \Delta h^2 M, \tag{18}$$

where M is the number of grid points where $|\phi_{j,l}^{n}| < \varepsilon$. For the time step of the iteration $\Delta t = \Delta h/10$ was chosen.

4. Premixing Experiment Simulation

For the analysis of our combined single-multiphase flow model the QUEOS premixing experiment Q08 [5] has been chosen. In this experiment molybdenum spheres with a diameter of 4.2 mm and a total mass of 10 kg were discharged from a height of 1.3 m through a tube into a water filled vessel with an inner cross section of 70 cm x 70 cm and a height of 138 cm. The spheres jet diameter was 9 cm and the spheres entered the water at a velocity of 5.12 m/s and a phase presence probability of 0.17. The water level in the vessel was 100 cm.

To get a qualitative impression of the premixing process two characteristic images of the experiment - one taken from the "North" side (with back-lighting) and the other from the "West" side (with black background) - are shown on Fig. 1. On Fig. 2 the pressures measured in the vessel at different levels are presented. Pressure $p1$ was measured in the gas space above the water level and shows the barometric pressure, whereas the other pressures were measured in water therefore showing also the static head according to their position. Pressure $p2$ and $p3$ were measured at the position 838 mm, $p5$ at the position 450 mm and $p6$ at the position 250 mm above the bottom of the vessel. The pressure rise after 0.5 s of the spheres release indicates the entry of the first spheres in the water and the pressure peak after 0.76 s the collapse of the gas chimney.

In the experiment simulation only the part of the vessel filled with water together with a 20 cm wide air zone over the water surface has been modelled. All other experiment features

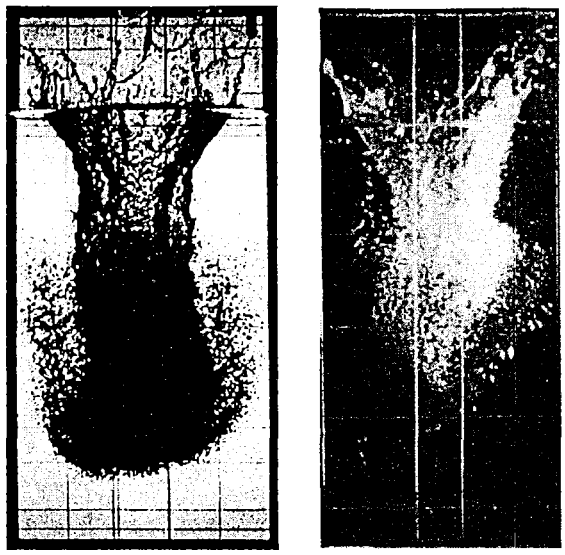

Fig. 1: Image of the experiment from the "North" (back lighting) and "West" (black background) side after 217 ms and 180 ms of the water surface impact.

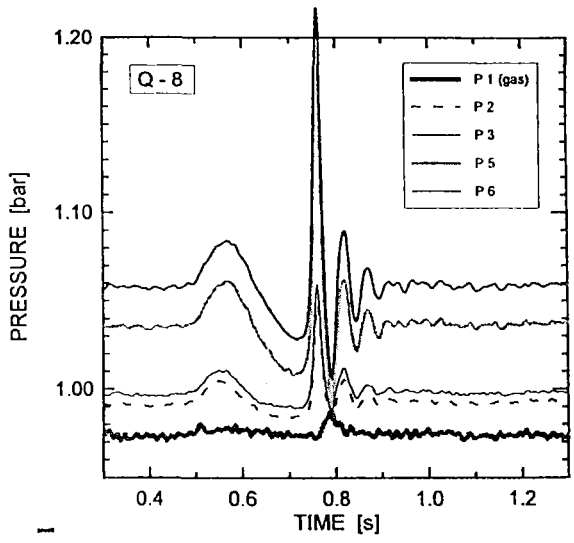

Fig. 2: Pressures measured in the vessel at different levels (p2, p3: 838 mm, p5: 450 mm and p6: 250 mm above the bottom of the vessel).

have been taken into account with appropriate boundary conditions. The experiment simulation has been performed in the cylindrical coordinate system presuming axial symmetry of the problem. This was not really the case in the experiment since the release mechanism with two doors opening along one dimension caused especially at the front of the spheres cloud an initially not axial symmetric distribution of the falling spheres (Fig. 1). To match the cross-sectional area of the vessel an equivalent radius of 41 cm was used in the axial symmetric model. The falling spheres were introduced in the model with boundary conditions. The appropriate boundary conditions for the spheres velocity and the spheres presence probability at the upper edge of the simulated region 20 cm above the water surface were determined from the known values at the water surface ($v_{zs} = 5.12\,m/s$, $\alpha_s = 0.17$) as

$$v_{zs}^b = \sqrt{v_{zs}^2 - 2gh} = \sqrt{5.12^2 m^2/s^2 - 2 \cdot 9.81 m/s^2 \cdot 0.2m} = 4.72 m/s,$$
$$\alpha_s^b = \alpha_s \frac{v_{zs}}{v_{zs}^b} = 0.17 \frac{5.12 m/s}{4.72 m/s} = 0.184. \tag{19}$$

The time interval the spheres are falling through the upper boundary of the simulated region was established from the total spheres mass and the calculated spheres mass flow rate

$$t^b = \frac{m_s}{\phi_{ms}} = \frac{4 m_s}{\alpha_s \rho_s \pi d^2 v_{zs}} = \frac{4 \cdot 10kg}{0.17 \cdot 10200 kg/m^3 3.14 \cdot 0.18^2 m^2 5.12 m/s} = 4.43 \cdot 10^{-2} s. \tag{20}$$

After that time the spheres presence probability at the upper boundary is zero $\alpha_s^b = 0$ and the boundary condition for the spheres velocity is the same as for the common water-air phase

$$\frac{\partial v_{rp}}{\partial z} = 0, \frac{\partial v_{zp}}{\partial z} = 0. \tag{21}$$

The experiment simulations have been performed in the cylindrical coordinate system on a mesh 41 x 120 grid points. So the grid spacing was exactly 1 cm, which is adequate for such kind of simulations as the convergence analysis showed. The continuity (1), momentum (2) and level set equation (10) were solved using the second order accurate high-resolution method based on the first order accurate upwind method and the second order accurate Lax-Wendroff method. The pressure equation was solved using the CGSTAB method [6].

5. Results of the Simulations

To get a better insight of the advantages of the level set method for free surface problems the water-air surface was in comparison calculated also with the second order accurate high-resolution method and the first order accurate upwind method. The results of the simulations are presented on figures 3-5. The first three pictures on Fig. 3 show the water presence probability in the cylindrical coordinate system after 218 ms of the water surface impact calculated with the level set, high-resolution and upwind method. The contours correspond to 0.01, 0.05, 0.1, 0.2, ... value. As expected the water-air surface remains sharp only at the level set method calculation, whereas the upwind method produces the strongest unphysical water-air mixing. The right picture represents the spheres presence probability intensity, which is defined as the integral of the spheres presence probability in view direction and is therefore directly comparable to the images in Fig. 1, with contours showing 0.002, 0.005, 0.01, 0.02, ... value. Since the selection of the numerical method for the water-air surface calculation has a minor influence on the spheres presence probability development only the result of the level set method calculation is presented.

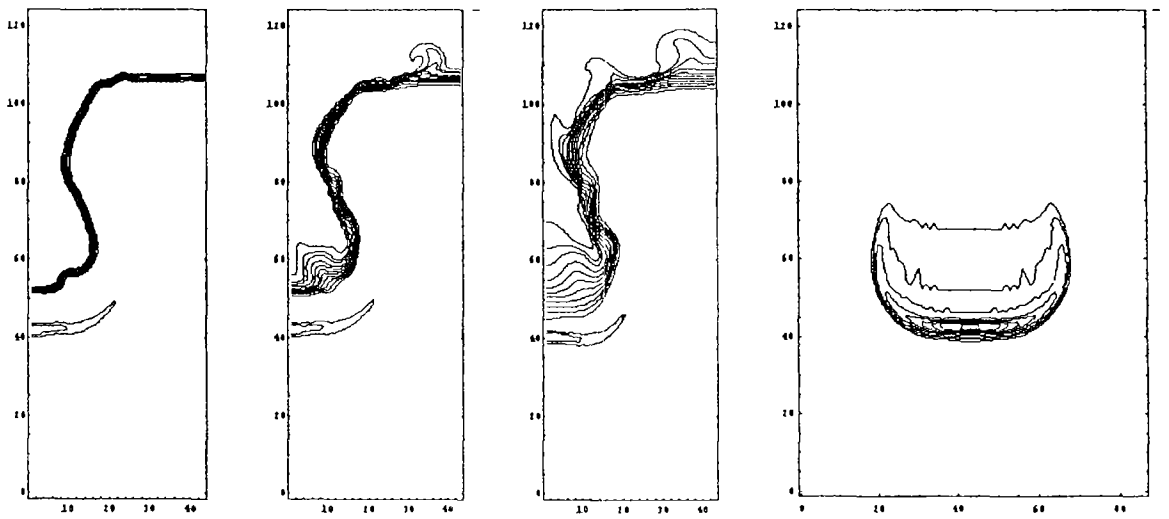

Fig. 3: Water presence probability in the cylindrical coordinate system calculated with the level set, high-resolution and upwind method, and the spheres presence probability intensity in the rectangular coordinate system for the level set method calculation after 218 ms of the water surface impact.

During all simulations also the pressure has been traced. In the first set of simulations all three phases, the water, the air and the spheres phase, have been treated as incompressible. The pressure curves for the upwind, high-resolution and the level set method calculation are shown on Fig. 4, where for clarity only the pressures $p2$ and $p6$ are presented. Since the simulation started 0.04 s before the spheres enter the water the time axis had to be shifted for 0.46 s to get the same time axis as on Fig. 2, where the time is measured after the release of the spheres, that is 0.5 s before the water surface impact. In the simulation the ambient pressure at the upper boundary was set to 1 bar, whereas in the experiment the average gas pressure was 0.975 bar (Fig. 2). So a pressure difference of 0.025 bar has to be considered when comparing the measured and calculated pressure values. As seen on Fig. 4 the pressure produces a spike when the gas chimney collapses, most pronounced at the level set method, whereas the pressure oscillations, which where observed in the experiment (Fig. 2), do not

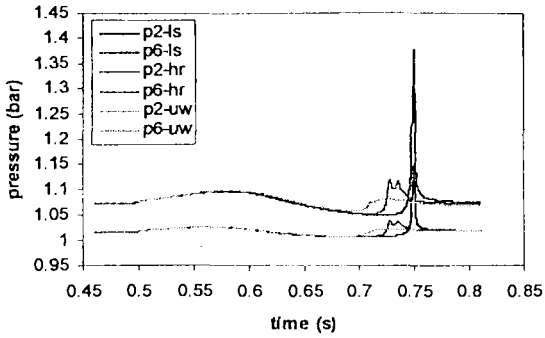

Fig. 4: Calculated pressures in the vessel at different levels for the upwind, high-resolution and level set method simulation for the incompressible case.

occur. This qualitatively different pressure behaviour is due to the incompressible air treatment in our model, since the reason for the pressure oscillations are the expansion and compression of the whole big air bubble, which forms after the air chimney collapse.

In the second series of simulations the air phase was therefore treated as compressible. Since the energy equation was not taken into account the correct air compressibility, which lies somewhere in the range bounded with the maximum isothermal and the minimum adiabatic value, has to be determined. A simple estimation shows that the heat diffusion in the air bubble during one oscillation period is negligible

$$\frac{dT}{\Delta T} = \frac{\lambda\, dt}{\rho c_p \Delta l^2} = \frac{257 \cdot 10^{-4}\, W/Km \cdot 0.06s}{1.29 kg/m^3 \cdot 1000 J/kgK \cdot 0.1^2 m^2} \approx 10^{-4} << 1 \qquad (22)$$

and that consequently the adiabatic compressibility is a very good approach. Despite of that the simulation has been performed also with the isothermal compressibility, above all to establish the compressibility influence on the results. The pressure behaviour in the compressible case taking into account the isothermal and the adiabatic compressibility is presented on Fig. 5. As expected pressure oscillations occur and they are most pronounced at the level set method, where the water-air surface remains sharp.

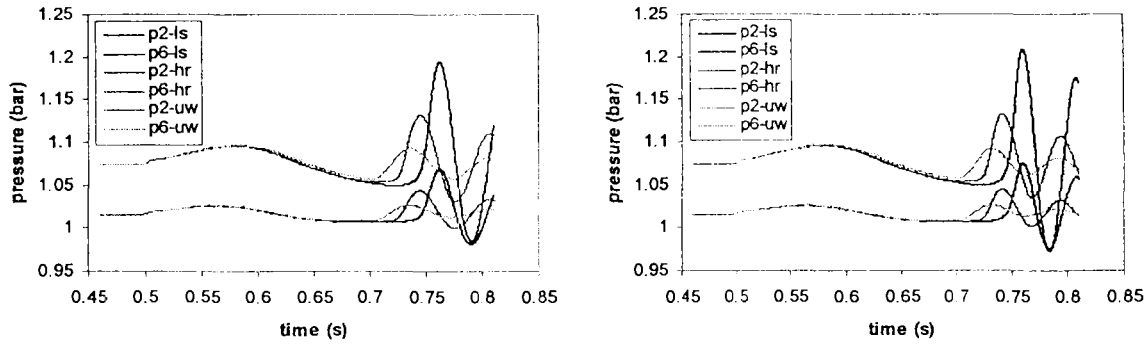

Fig. 5: Calculated pressures in the vessel at different levels for the upwind, high-resolution and level set method simulation considering the isothermal (left side) and adiabatic (right side) air compressibility.

To make the comparison of the simulations easier the main results are assembled in table 1. The maximum pressure difference between $p6$ and the ambient pressure, the time when the pressure peak is reached and the time interval between the first pressure maximum and minimum during the pressure oscillations are listed for all presented simulations. The experimental values are also added for completeness and as a reference but not for rigorous comparison since the experimental conditions were different.

The reason for so various pressure behaviour at the upwind, high-resolution and level set method calculation is the different extend of water-air surface spreading these numerical methods produce. The upwind method produces the highest spreading, so the air chimney starts to close the fastest. Since the density of the spread water-air surface changes gradually also the pressure rise is the lowest. The high-resolution method produces a sharper water-air

interface; therefore the amplitude of the pressure oscillations is greater. The small oscillations appearing in the pressure in Fig. 4 are not real oscillations, since they originate in the closure of the air chimney at two different points at nearly the same time. The pressure changes are highest at the level set method since it remains the water-air interface sharp during the whole simulation like it was observed also in the experiment. As expected the compressibility has a direct influence on the pressure oscillating frequency, which is higher for the lower adiabatic compressibility.

	Exp.	Simulation								
		Incompressible			Isothermal			Adiabatic		
		LS	HR	UW	LS	HR	UW	LS	HR	UW
Δp_{max} (bar)	.244	.376	.119	.080	.194	.132	.093	.209	.133	.092
t_{pmax} (s)	.760	.750	.728	.723	.762	.745	.735	.760	.741	.731
$\Delta t_{osc}/2$ (s)	.030	/	/	/	.028	.031	.037	.024	.027	.031

Table 1: Main results of the incompressible and compressible simulations with different numerical methods together with the experimental measurements.

6. Conclusions

A new concept of multiphase flow treatment, the combined single-multiphase flow formulation, has been presented and applied to isothermal premixing experiments. The idea of the combined single-multiphase flow formulation is to treat the phases, which remain separated by a free surface (water and air) as a single phase with discontinuous phase properties, whereas the other phases (spheres) are treated as usually with a multiphase flow model. The free surface (water-air interface) has been determined with the front capturing level set method, which is widely used in the last years.

For the analysis of the combined single-multiphase flow model the QUEOS premixing experiment Q08 has been chosen. A number of simulations has been performed using different numerical methods for the water-air surface determination (level set, high-resolution and upwind) treating the air as compressible or incompressible.

As expected the results of the simulations showed that the water-air surface remains sharp only at the level set method calculation and that the upwind method produces the highest spreading. Consequently the pressure variations are highest for the level set method where the density at the water-air interface changes most rapidly. The pressure oscillations, which were observed in the experiment, could be reproduced only in the compressible case since they are a consequence of the entrapped air bubble oscillations.

7. References

[1] B.D. Turland, G.P. Dobson: *Molten Fuel Coolant Interactions: A state of the art report*, European Commission, Nuclear Science and Technology, Luxembourg, 1996.

[2] M. Leskovar, B. Mavko: *ESE a 2D Compressible Multiphase Flow Code Developed for MFCI Analysis – Code Validation*, Nuclear Energy in Central Europe '98, Čatež, 1998, pp. 319-326.

[3] D.F. Fletcher, P.J. Witt: *Numerical Studies of Multiphase Mixing with Application to some Small-Scale Experiments*, Nuclear Engineering and Design, 1996, pp. 135-145.

[4] Y.C. Chang, T.Y. Hou, B. Merriman, S. Osher: *A Level Set Formulation of Eulerian Interface Capturing Methods for Incompressible Fluid Flows*. Journal of Computational Physics, 124, 1996, pp. 449-464.

[5] L. Meyer, G. Schumacher: *QUEOS, a Simulation-Experiment of the Premixing Phase of a Steam Explosion with Hot Spheres in Water, Base Case Experiments*. FZKA Report 5612, Forschungszentrum Karlsruhe, 1996.

[6] J.H. Ferziger, M. Perič: *Computational Methods for Fluid Dynamics*. Springer-Verlag, Heidelberg, 1996.